Hot-Pressed Super-Elastic Graphene Aerogel with Bidirectional Thermal Conduction Properties as Thermal Interface Materials

Peng Lv *, Xiaofeng Zhou , Songyue Chen

Posted Date: 6 November 2023

doi: 10.20944/preprints202311.0290.v1

Keywords: thermal interface materials; graphene; hot-pressing; thermal annealing; bidirectional

Article

Hot-Pressed Super-Elastic Graphene Aerogel with Bidirectional Thermal Conduction Properties as Thermal Interface Materials

Peng Lv *, Xiaofeng Zhou and Songyue Chen

College of Electronic and Optical Engineering & College of Flexible Electronics (Future Technology), Nanjing University of Posts and Telecommunications, Nanjing 210023 China; xfzhou@njupt.edu.cn (X.Z.); sychen@njupt.edu.cn (S.C.)

* Correspondence: lvpeng1028@163.com; Tel.: +86-25-8586-6296

Abstract: Traditional graphene-based films normally possess high thermal conductivity (TC) only along single direction, which is not suitable for thermal interface materials (TIMs). Here, a graphene film with excellent bidirectional TC and mechanical properties was prepared by hot-pressing super-elastic graphene aerogel (SEGA). Thermal annealing at 1800℃ improves the further restacking of graphene sheets, bring the SEGA high structure stability for enduring the hot-pressing process. The junctions and nodes between the graphene layers in the hot-pressed SEGA (HPSEGA) film provide bidirectional heat transport paths. The in-plane TC and through-plane TC of HPSEGA film with thickness of 101μm reach 740 $Wm^{-1}K^{-1}$ and 42.5 $Wm^{-1}K^{-1}$, respectively. In addition, HPSEGA film with higher thickness still maintains excellent thermal transport properties due to the interconnected structure reducing the effect of the defects. The infrared thermal images visually manifest the excellent thermal-transfer capability and thermal dissipation efficiency of the HPSEGA films, indicating the great potential as advanced bidirectional TIMs.

Keywords: thermal interface materials; graphene; hot-pressing; thermal annealing; bidirectional

1. Introduction

With the rapid development of 5G communication and artificial intelligence, the high-power and highly integrated devices generate ultra-high heat-flow density during the operation, making the performance, reliability and lifetime of electronics decline [1,2]. Thermal interface materials (TIMs) are widely used to bridge between the heat source and the heat sink to eliminate temperature. Graphene with extraordinary intrinsic thermal conductivity (TC) of 3500-5300 $Wm^{-1}K^{-1}$ and excellent mechanical strength is regarded as one of the most potential TIMs [3,4].

To date, many studies have focused on the highly thermal-conductive graphene films (GFs) normally assembled from graphene oxide (GO) sheets. GO film can be easily prepared by casting [5], vacuum filtration [6], electro-spray deposition [7] or evaporation-induced assembly [8] of GO solutions. And then highly thermal-conductive GFs can be obtained by further reduction, carbonization, graphitization and mechanical compression of GO films [9]. During the preparation process, the graphene sheets trend to orientate and distribute along single direction especially under the high pressure [10]. Sp^2-hybridized carbon atoms allow for efficient phonon transport through the lattice oriented along the in-plane direction [11]. Thus, GFs composed of layer-by-layer stacked graphene sheets possess excellent in-plane TC (Table 1), which can be commercially used as high-performance heat spreader in thermal management system [12]. However, the weak Van Der Waals coupling between graphene layers causes serious phonon scattering in the direction perpendicular to the lattice plane, leading to those conventional graphene films showing a through-plane TC 2-3 orders of magnitude lower than that in the in-plane direction [13–15]. Conventionally, TIMs are applied to enhance the thermal conduction between the mating surfaces. To maximize the heat transfer efficiency, TIMs are required to possess not only high in-plane TC but also improved through-plane TC [16]. Some studies for the fabrication of vertically aligned structure of graphene

 doi:10.20944/preprints202311.0290.v1

have been reported [13,17–21], showing ultra-high through-plane TC (up to 615 $Wm^{-1}K^{-1}$) [22]. But they are still not suitable for TIMs, due to the sacrificed in-plane TC and high contact thermal resistance arising from the surface rigidity of vertical graphene [23].

Creation of an axial thermal transfer pathway for the construction of a 3D thermal conductive network is considered as a key milestone that could further extend the applications of GFs in TIM filed. Researchers attempted to introduce nanoparticles (such as Cu nanoparticles [24], Au nanoparticles [25] and SiO_2@C nanoparticles [26]) or 1D nanomaterials (such as carbon nanotubes [14,27–29], SiC nanorod [30], carbon nanoring [31]) into interlayer of graphene sheets to enhance the heat conduction in the through-plane direction. But the intercalation of nanoparticles inevitably induces decreased densities and increased deficiencies, which leads to the decrease of in-plane TC. And during the directional compression, 1D nanofillers tend to orient in the direction horizontal to graphitic lattice plane, leading to structure damage of the thermal transport bridge. Thus, it is still a major challenge to design a novel structure of GFs for improving the TC values both in in-plane direction and through-plane direction.

Table 1. TC, thickness and density of the highly thermal-conductive graphene-based films reported in references.

Highly thermal-conductive graphene-based films	In-plane TC ($W\ m^{-1}\ K^{-1}$)	Through-plane TC ($W\ m^{-1}\ K^{-1}$)	Thickness (μm)	Density ($g\ cm^{-3}$)
High TC in single direction				
Graphene paper [7]	1434	-	-	2.1
Graphene-based hybrid film [8]	1597	2.65	7	-
GF [33]	1940	-	10	2.03
GF [34]	1043.5	-	-	-
Ultra-thin GF [35]	3200	-	0.8	2.1
GF [36]	1100	-	8.1	
Large-sized GF [37]	803.1	3.98	14	2.05
Ball-milling exfoliated graphene paper [38]	1529	-	30	1.8
Glucose modified GF [39]	1300	-	-	-
Electrochemically exfoliated graphene paper [40]	1022.8	-	-	-
Bidirectional high TC				
Vertical carbon nanotube@SiC-graphene film [14]	397.9	41.7	200	-
Graphene/nanocopper film [24]	234.9	5.22	-	-
Graphene-SiO2@C film [26]	36.54	6.65	-	-
Graphene-carbon nantube [27]	933.37	6.27	106	0.985
Graphene-carbon nanotube-graphite film [28]	182.6	32.96	6000	1.67
Graphene hybrid paper [30]	263	17.6	500	0.8
Carbon Nanoring/Graphene Hybrid Paper [31]	890	5.81	-	-
This work	740.3 688.1	42.5 39.6	101 192	1.35 1.57

In addition, according to Fourier's low, both high TC and enlarged thickness (determines the cross-sectional area) are desirable in maximizing the heat transfer capability at the in-plane direction of the TIMs [10,27,32]. Nevertheless, the high TC is demonstrated only with extremely thin GFs less than 30μm (Table 1). As the thickness increase, the multiple grain boundary defects of the GFs increase, leading to the declining of TC. It less favored ultrahigh thermal flux equipment (102-106 W cm^{-2}) than the metal-based TIMs [27]. The GFs with bidirectional superior thermal conduction

 doi:10.20944/preprints202311.0290.v1

performances and high heat flux hasn't been reported. Hence, it is still a great challenge to fabricate high thick GFs without sacrificing overall thermal properties.

Herein, the super-elastic graphene aerogels (SEGAs) were fabricated by ice template method and thermal annealing process (1800°C). The SEGAs can maintain the continuously interconnected structure even at ultra-high compressive strain due to the thermal treatment improving the toughness of the cell walls. Then the SEGAs were hot-pressed at 30-50 MPa and 1800°C to form the hot-pressed SEGA (HPSEGA) films (Figure 1) with dense structure and interconnected morphology. In the HPSEGA, there are continuous thermal transport paths between adjacent graphene layers without any nanoparticles or 1D nanofillers, which eliminates the interface thermal resistance in the films. In addition, the thick HPSEGA film with a thickness up to 192μm can be obtained by hot-pressing thick SEGA. Because of the low interface thermal resistance and dense structure, the HPSEGA thick film achieves high heat flux and excellent bidirectional superior thermal transport performances of in-plane and through-plane. And the advanced thermal interfacial performances of the HPSEGA films are directly certified by thermal infrared imaging. Our works provides a novel way to prepare high-performance bidirectional GF TIMs with high heat flux.

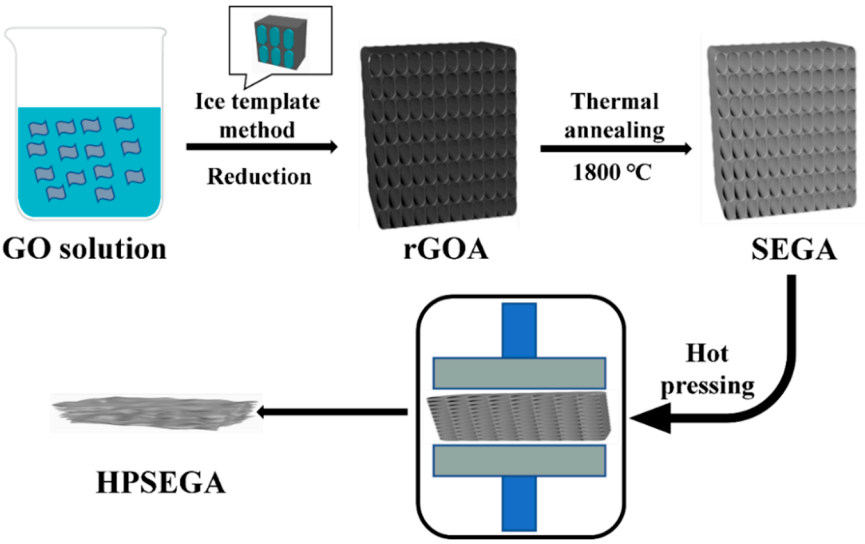

Figure 1. The schematic drawing of preparation of HPSEGA film.

2. Materials and Methods

2.1. Preparation of HPSEGA film

Graphene oxide (GO) dispersion was prepared by the modified Hummers method. The reduced GO aerogel (rGOA) was self-assembled by the ice template method according to the previous process [30]. In a typical synthesis procedure, GO aqueous solution with L-ascorbic acid was heated at 90°C for 20 min to produce partially reduced GO hydrogel. Then the hydrogel was treated by the freeze-thaw process at -18 °C and room temperature. A further reduction process was carried out for 8h at 95°C using initial L-ascorbic acid. After drying at 50°C, the rGOA was prepared. For obtaining the SEGA, the rGOA was thermal annealing at 1800°C under vacuum condition to form tightly packed graphene cell walls with improved mechanical robustness. Subsequently, the HPSEGA films were obtained by hot-pressing at 1800°C and 10 MPa under vacuum condition for 1h.

2.2. Characterization

The micro-morphologies of the samples were observed by a field-emission scanning electron microscope (SEM, Hitachi S4800, Japan) system at 10 KV. Compressive stress/strain measurements of SEGA and tensile test of HPSEGA films were carried out on a single-column system (Instron 5843, USA) equipped with 1 KN load cell. The crystal structure was investigated by X-ray diffraction (XRD, D8 Advance, Bruker, Germany) using Cu Kα1 radiation (λ=1.54 Å) with a scan rate of 4°/min. X-ray

 doi:10.20944/preprints202311.0290.v1

photoelectron spectroscopy (XPS, Physical Electronics, PHI-5300, USA) spectra were collected with a monochromatic Mg Ka radiation at a voltage of 14 kV and a power of 250 W. The in-plane and through-plane TC values of the films were calculated from the following formula:

$$\kappa = \alpha \rho C_p \quad (1)$$

where κ, α, ρ and C_p are the TC, thermal diffusivity, density and specific heat capacity of the films, respectively. The thermal diffusivity (α) was determined by a laser flash apparatus (LFA 467, Netzsch, Germany), the specific heat capacity (C_p) was determined by a differential scanning calorimeter (Q20, TA instruments, USA), and the density (ρ) was measured using the water displacement method. The infrared thermal imager (Ti32, Fluke, USA) was used to record the temperature distribution images of the samples.

3. Results and discussion

Figure 2a displays the rGOAs and SEGAs, respectively. The shape and size of the aerogels depend on the utilized reactor during the ice-template process. It can be found that, after 1800°C thermal annealing process, the color of the aerogels turns from black to silvery metallic luster, indicating the full repair of defects of rGO sheets. Figure 2b shows the micro-structure of the SEGAs at the cross-section view, which presents oriented cellular and honeycomb-like architecture. Each cell walls are composed of tightly stacked graphene sheets and converge at the junctions or nodes (Figure 2c). The SEGAs with 3D interconnected network is significantly different from the rGO films with parallel structure used for preparing the highly thermal-conductive GF films. The interconnected cell walls are in favor of decreasing interface contact thermal resistance in the aerogels and provide continuous thermal transport path along the network. As shown in Figure 2d, the SEGA can be squeezed into pellet under a pressure of 10 MPa. Once the external pressure is removed, the SEGA can almost completely recover to its original shape rapidly. In contrast, the rGOA deforms permanently indicating a structural collapse (Figure S1). SEGAs with various densities (1.8~7.2 mg cm^{-3}) were prepared by controlling the GO concentrations (Figure S2e). As shown in Figure S2a-d, with increasing GO concentration, the porous structure becomes denser and the average pore size is smaller, while the oriented cellar structure of SEGA maintains well. The strain/stress curves of the SEGAs with various densities are shown in Figure 2e, indicating the recoverable compressive strain can reach 99%. The strain-stress curves for 100 cycles (Figure S2f) indicate the structure stabilization of SEGA. Higher compressive strain (>99%) of the sample can't be measured accurately due to the limitation of the equipment sensitivity. The high compressibility arises from mechanical robustness of tightly packed cell walls and regular cellular structure of the SEGAs. And this ultra-high structure stability is crucial for preparing GF films with interlayer junction structure and bidirectional heat transport path even after the hot-pressing process.

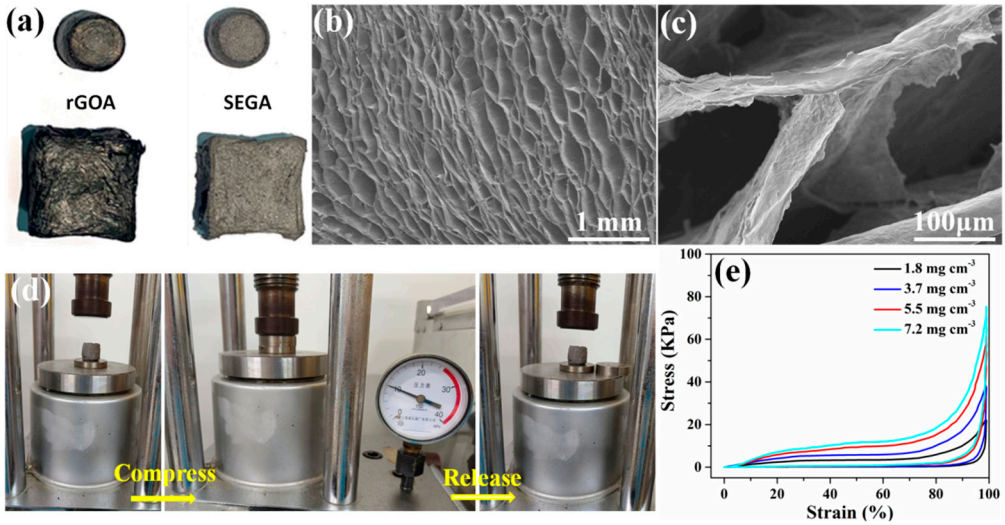

 doi:10.20944/preprints202311.0290.v1

Figure 2. (a) Digital images of rGOAs and SEGAs, respectively; (b, c) SEM images of cross-section of SEGA; (d) Real-time photos of the compression-recovery process of SEGA; (e) Compressible stress-strain curves of SEGAs with various densities.

As shown in Figure 3a, the HPSEGA films prepared by hot-pressing SEGA are smooth, flexible and uniform with a silvery metallic luster. The micro-structure of the surface of HPSEGA film shows a complete continuous surface (Figure 3b). As shown in the cross-sectional SEM in Figure 3c, a HPSEGA thin film shows a thickness of 101μm, which is prepared by hot-pressing a 2cm thick SEGA with a density of 7.2 mg cm^{-3}. The density of this HPSEGA film reaches 1.35 g cm^{-3}. It can be found that the graphene layers trend to orient perpendicularly to the pressure direction, which provides a pathway for in-plane phonon transports. High magnification SEM images indicate that the junctions and nodes between the adjacent graphene layers still maintains well even after hot-pressing process (marked with circles in Figure 3d,e). This interconnected structure is significantly different from the typical layered structure of the traditional GFs prepared from the GO films (Figure S3). Those junctions and nodes in HPSEGA films act as the "bridges" to connect adjacent graphene sheets in the vertical direction, which can effectively improve the through-plane TC. In addition, a thicker HPSEGA film (192μm) exhibited similar structure (Figure 3f) can be obtained by hot-pressing thicker SEGA (4cm). This thicker film possess higher density (1.57 g cm^{-3}) than that of the thinner HPSEGA film (101 μm), which may be attributed to more effective stress load for thicker SEGA during the hot-pressing process. We envision that HPSEGA films with much higher thickness can be easily achieved by just increasing the thickness of the SEGAs.

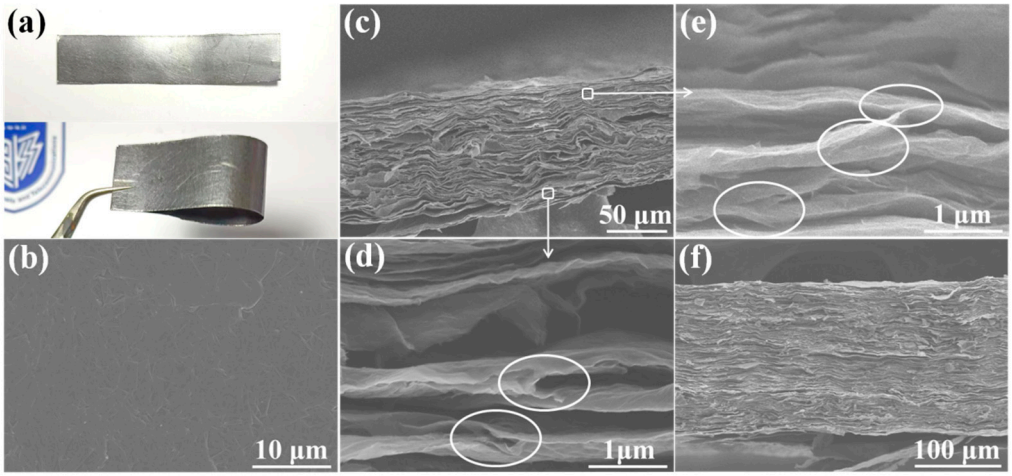

Figure 3. (a) Digital image of HPSEGA films; (b) SEM image of the surface of HPEGA film; Cross-sectional SEM morphology of the HPSEGA thin film (c-e) and the HPSEGA thick film (f).

The structure change can be characterized by XPS and XRD. As shown in XRD patterns in Figure 4a, rGOA, SEGA, HPSEGA film shows the typical peaks at the 2θ value of 26.53°, 26.62° and 26.71° corresponding to the d-spacing of 3.53Å, 3.45Å and 3.36Å. The observed changes in XRD peak features implies that thermal annealing process improves the further restacking of graphene sheets. As shown in the XPS spectra (Figure 4b), the O1s peaks of SEGA and HPSEGA film become negligible, and the carbon to oxygen (C/O) atomic ratio of rGOA is 4.66, and promotes remarkably to 71.21 and 76.43 for SEGA and HPSEGA film, confirming a virtually complete elimination of oxygen functional groups after thermal annealing. The sharp and pronounced C=C/C-C peaks of SEGA and HPSEGA indicates the significant restoration of sp2 bonded carbon lattice structure (Figure 4c).

 doi:10.20944/preprints202311.0290.v1

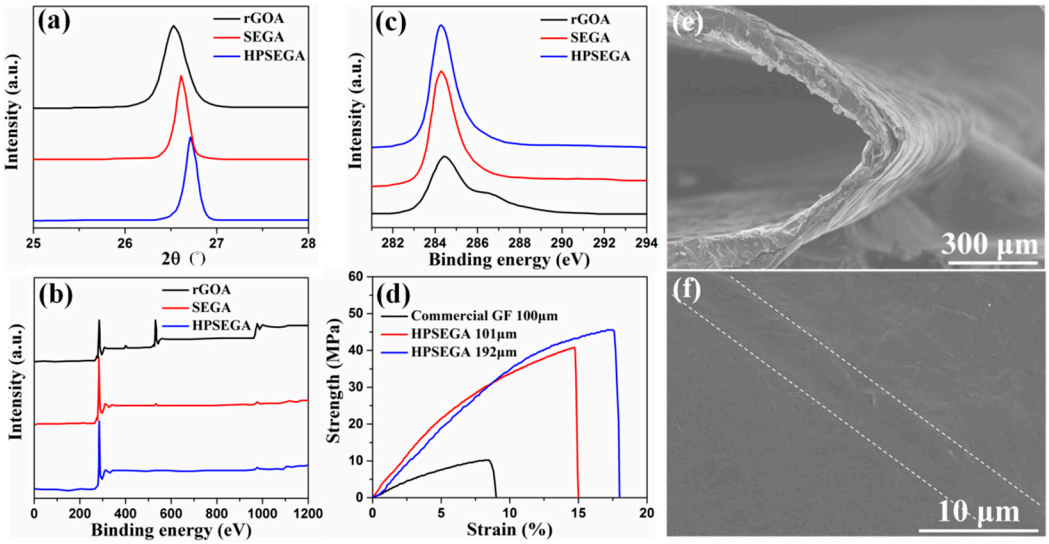

Figure 4. (a) XRD spectra, (b) XPS spectra, and (c) C1s of the rGOA, SEGA, and HPSEGA film, respectively; (d) Stress-strain curves of the films; SEM images of (e) cross section view of HPSEGA film under 135° bending and (f) surface morphology change of HPSEGA film after bending test.

The mechanical performances of the HPSEGA films have been investigated. A commercially-available GF (Hefei AOQI Electronic Technology Co., Ltd, GSH-T100, 100μm thick) was also tested for a comparison. Figure 4c shows the stress-strain curves of the films under a tensile stress. HPSGA film with thickness of 101μm shows a strain 15% of under 39.8MPa of tensile stress. At a given strain value, the HPSEGA films can endure about 3 times larger stress compared with the commercial GF. And the HPSEGA film possesses higher tensile stress and strain. To demonstrate the flexible properties of HPSEGA film, bending tests were performed. From Figure 4e, HPSEGA film can maintain structure stability under 135º bending. It exhibits excellent flexibility and reliability after 10 cycles bending/releasing with slight wrinkles (Figure 4f). Nonetheless, clear breakages appear on the surface of commercial GF (Figure S4).

This strong mechanical property of HPSEGA is attributed to the interconnected cross-linked structure between graphene layers. This special structure can maintain well even under hot-pressing is attributed to two factors: 1. Thermal annealing of SEGA at 1800°C improves the π-π interaction between the graphene sheets in the cell walls, leading to larger mean size of ordered stacking of graphene and bring the cell walls high toughness and mechanical robustness. Thus, SEGA possess a high structure stability to bear the hot-pressing process. 2. In the previous literatures, the thermal annealing process (2600-2800°C) and the cold-pressing process (50-300 MPa) were carried out individually to prepare GFs [9,10,35,37,40]. According to the theory of "stress graphitization"[42], pressure-induced effect accelerates the transformation of incommensurately-stacked carbon to graphite. Thus, lower pressure (10 MPa) and lower annealing temperature (1800°C) is needed during the hot-pressing process in this work. And the relative low pressure and temperature are in favor of maintaining the interconnected structure between graphene layers during the preparation process.

The TC values of HPSEGA films have been measured. As shown in Figure 5a, HPSEGA film with thickness of 101μm exhibits in-plane TC of 740.3 $Wm^{-1}K^{-1}$ and through-plane TC of 42.5 $Wm^{-1}K^{-1}$. In comparison with the GFs listed in Table 1, especially those with high bidirectional TC values, HPSEGA films show excellent combination thermal transport capability. For example, compared with graphene/carbon nanotube film [27], HPESGA film with the similar thickness (~100μm) possesses a relatively low in-plane TC, but its through-plane TC is ~7 times higher than that of graphene/carbon nanotube film. And HPSEGA film with thickness of 192μm shows slightly lower through-plane TC (39.6 $Wm^{-1}K^{-1}$) than that of vertical carbon nanotube@SiC-graphene hybrid film [14], whereas its in-plane TC (688.1 $Wm^{-1}K^{-1}$) is 1.7 times higher than that of the hybrid film. The HPSEGA film achieves two directions of the heat dissipation mechanism as follows. Firstly, the graphene sheets arrange horizontally and play a dominant role at in-plane phonon transport, which

 doi:10.20944/preprints202311.0290.v1

is related to the in-plane TC. Secondly, the junctions and nodes effectively connect the graphene layers in the vertical direction, which mainly contribute to the channels for through-plane phonon transports. As mentioned above, normally the TC values of GFs decline significantly with the thickness enlargement due to the increase of defects. However, HPSEGA film with higher thickness (191μm) still shows high TC values in both in-plane and through-plane direction, which is attributed to that the interconnected structure provide more heat path and reduce the effect of the defects in the film.

The heat transfer capability of the thermal conductive films was characterized by infrared thermal images (Figure 5b). The commercial thin GF (100μm, in-plane TC=800 $Wm^{-1}K^{-1}$, through-plane TC=10 $Wm^{-1}K^{-1}$), commercial thick GF (200μm, in-plane TC=500 $Wm^{-1}K^{-1}$, through-plane TC=5 $Wm^{-1}K^{-1}$), HPSEGA film (101μm) and HPSEGA film (192μm) were caught in the middle of a constant temperature heat source. It is obvious that the thick films show more uniform temperature distribution, even though the thin films holed higher TC. It reveals the intrinsic thickness of a thermally conductive material is crucial to its heat flux in practical applications. In addition, the brighter top-end image of HPEAG film (192μm) means higher surface temperature and indicates higher heat-transfer efficiency in comparison with the commercial thick GF (200μm), which is attributed to both high TC values and thickness.

Figure 5c presents a schematic of different GFs as the TIMs. In horizontal GF and vertical GF, the aligned graphene chains provide thermally conductive pathway array only along single direction. None of them are not ideal TIMs. But HPSEGA film with bidirectional thermally conductive can significantly enhance the heat dissipation effect between heat source and heat sink. Utilizing the highly bidirectional TC of HPSEGA, we demonstrated its use as a TIM for heat dissipation of a high-power LED lamp (Figure 5d,e). For comparison, commercial GF was also used (Figure 5h,i). The films were mounted between an aluminum heat sink and a high-power LED (Figure 5e). Infrared thermal imager was used to monitor the temperature change. It can be seen from Figure 5f–i that the temperatures of the LED with HPSEGA film (101μm) as TIM are 68.7°C and 25.0°C lower than that with commercial GF (192 μm) after 180s operation. These results demonstrate the great potential of the HPSEGA film for TIMs in thermal management system.

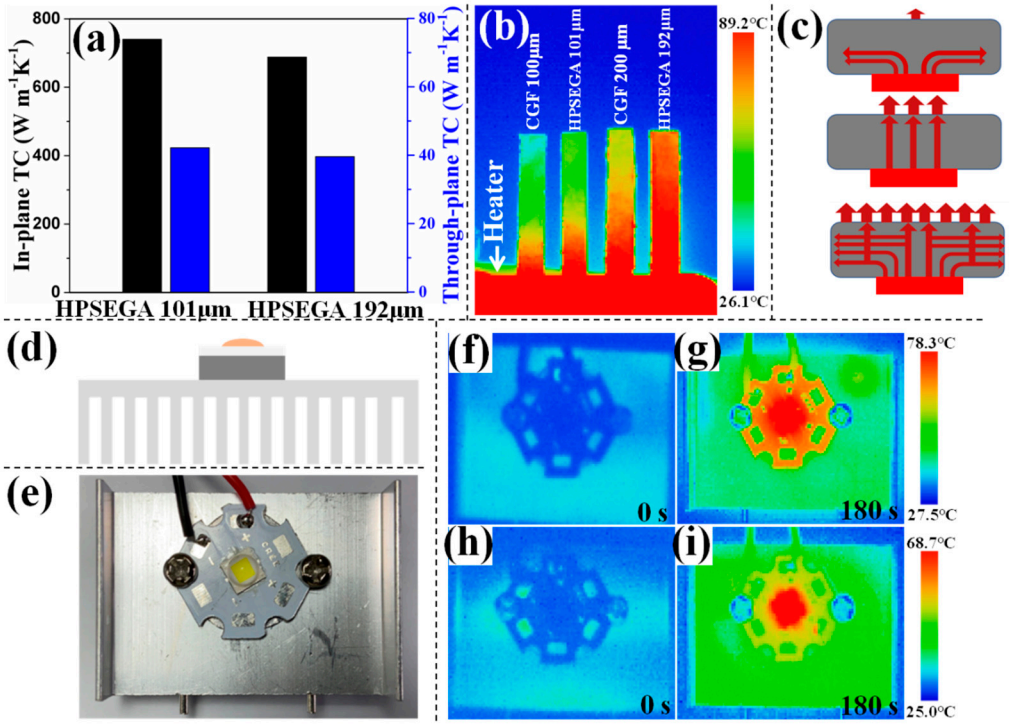

Figure 5. (a) TC values of the HPSEGA films; (b) Infrared thermal image of the films attached vertically on a constant temperature heat source; (c) Schematic diagram of the thermal transport mechanism in GF with horizontal structure, GF with vertical structure and HPSEGA film; (d) Schematic diagram and (e) photos of the LED devices, in which the films is mounted between the

LED and heat sink; (f-i) Infrared thermal images showing the heat dissipation of LED lamp with (f,g) HPSEGA film and (h,i) commercial GF as TIMs. The images were captured at (f,h) 0s and (g,i) 180s.

4. Conclusions

In summary, the HPSEGA film with both high in-plane TC and through-plane TC were prepared by hot-pressing the SEGA. The structure characterization results indicate that the thermal annealing process improves the further restacking of graphene sheets in cell walls, bring the SEGA high structure stability during the hot-pressing process. Micro-morphology characterization shows that the junctions and nodes between graphene layers can be maintained in HPSEGA film, which provides the heat transport path in both in-plane direction and through-plane direction. The HPSEGA films possess excellent bidirectionally thermal transport ability. The in-plane TC and through-plane TC of HPSEGA film (101μm) reach 740.3 Wm-1K-1 and 42.5 Wm-1K-1, respectively. Infrared thermal images visually manifest the advanced heat-dissipation efficiency of HPSEGA film as TIMs compared with the commercial GF. In addition, HPSEGA film with higher thickness (200μm) also possesses high bidirectional TC values due to its interconnected structure. By getting rid of the aging issue of conventional GF TIMs, the HPSEGA film with interconnected structure has great potential to be used as high performance TIMs with good thermal and mechanical stability.

Supplementary Materials: The following supporting information can be downloaded at the website of this paper posted on Preprints.org.

Author Contributions: P.L. conceived the idea and wrote the paper. X.Z. and S.C. carried out the sample fabrication and the measurements of the materials and devices.

Institutional Review Board Statement: Not applicable.

Informed Consent Statement: Not applicable.

Data Availability Statement: Not applicable.

Conflicts of Interest: The authors declare no conflict of interest.

References

1. Khan, J.; Momin, S. A.; Mariatti, M. A review on advanced carbon-based thermal interface materials for electronic devices. Carbon 2020, 168, 65-112. doi:10.1016/j.carbon.2020.06.012.
2. Zhang, F.; Feng, Y. Y.; Feng, W. Three-dimensional interconnected networks for thermally conductive polymer composites: Design, preparation, properties, and mechanisms. Materials Science & Engineering R. 2020, 142, 100580. doi:10.1016/j.mser.2020.100580.
3. Lv, L.; Dai, W.; Yu, J. H.; Jiang, N.; Lin, C. T. A mini review: application of graphene paper in thermal interface materials. New Carbon Mater. 2021, 36, 930-938. doi:10.1016/S1872-5805(21)60093-8.
4. Zhang, Y.; Heo, Y. J.; Son, Y. R.; In, I.; An, K. H.; Kim, B. J.; Park, S. J. Recent advanced thermal interfacial materials: A review of conducting mechanisms and parameters of carbon materials. Carbon 2019, 142, 445-460. doi:10.1016/j.carbon.2018.10.077.
5. Feng, C. P.; Chen, L. B.; Tian, G. L.; Wan, S. S.; Bai, L.; Bao, R. Y.; Liu, Z. Y.; Yang, M. B.; Yang, W. Multifunctional thermal management materials with excellent heat dissipation and generation capability for future electronics. ACS Appl. Mater. Interfaces 2019, 11, 18739-18745. doi:10.1021/acsami.9b03885.
6. Hou, Z. L.; Song, W. L.; Wang, P.; Meziani, M. J.; Kong, C. Y.; Anderson, A.; Maimaiti, H.; LeCroy, G. E.; Qian, H.; Sun, Y. P. Flexible graphene–graphene composites of superior thermal and electrical transport properties. ACS Appl. Mater. Interfaces 2014, 6, 15026-15032. doi:10.1021/am502986j.
7. Xin, G. Q.; Sun, H. T.; Hu, T.; Fard, H. R.; Sun, X.; Koratkar, N.; Borca-Tasciuc, T.; Lian, J. Large-area freestanding graphene paper for superior thermal management. Adv. Mater. 2014, 26, 4521-4526. doi:10.1002/adma.201400951.
8. Zou, R.; Liu, F.; Hu, N.; Ning, H. M.; Gong, Y. K.; Wang, S.; Huang, K. Y.; Jiang, X. P.; Xu, C. H.; Fu, S. Y.; Li, Y. Q.; Yan, C. Graphene/graphitized polydopamine/carbon nanotube all-carbon ternary composite films with improved mechanical properties and through-plane thermal conductivity. ACS Appl. Mater. Interfaces 2020, 12, 57391-57400. doi:10.1021/acsami.0c18373.
9. Yang, G.; Yi, H. K.; Yao, Y. G.; Li, C. W.; Li, Z. Thermally conductive graphene films for heat dissipation. ACS Appl. Nano Mater. 2020, 3, 2149-2155. doi:10.1021/acsanm.9b01955.

10. Chen, S. J.; Wang, Q. L.; Zhang, M. M.; Huang, R. Z.; Huang, Y. Y.; Tang, J.; Liu, J. H. Scalable production of thick graphene films for next generation thermal management applications. Carbon 2020, 167, 270-277. doi:10.1016/j.carbon.2020.06.030.
11. Malekpour, H.; Chang, K. H.; Chen, J. C.; Lu, C. Y.; Nika, D. L.; Novoselov, K. S.; Balandin, A. A. Thermal conductivity of graphene laminate. Nano Lett. 2014, 14, 5155-5161. doi:10.1021/nl501996v.
12. Liu, L.; Bian, X. M.; Tang, J.; Xu, H.; Hou, Z. L.; Song, W. L. Exceptional electrical and thermal transport properties in tunable all-graphene papers. RSC Adv. 2015, 5, 75239-75247. doi:10.1039/c5ra15533a.
13. Dai, W.; Ma, T. F.; Yan, Q. W.; Gao, J. Y.; Tan, X.; Lv, L.; Hou, H.; Wei, Q. P.; Yu, J. H.; Wu, J. B.; Yao, Y. G.; Du, S. Y.; Sun, R.; Jiang, N.; Wang, Y.; Kong, J.; Wong, C. P.; Maruyama, S.; Lin, C. T. Metal-level thermally conductive yet soft graphene thermal interface materials. ACS Nano 2019, 13, 11561-11571. doi:10.1021/acsnano.9b05163.
14. Peng, L.; Yu, H.; Chen, C.; He, Q.; Zhang, H.; Zhao, F.; Qin, M.; Feng, Y.; Feng, W. Tailoring dense, orientation-tunable, and interleavedly structured carbon-based heat dissipation plates. Adv. Sci. 2023, 10, 2205962. doi:10.1002/advs.202205962.
15. Li, Y. H.; Zhu, Y. F.; Jiang, G. P.; Cano, Z. P.; Yang, J.; Wang, J.; Liu, J. L.; Chen, X. H.; Chen, Z. W. Boosting the heat dissipation performance of graphene/polyimide flexible carbon film via enhanced through-plane conductivity of 3D hybridized structure. Small 2020, 16, 1903315. doi:10.1002/smll.201903315.
16. Zhou, Y.; Wu, S.; Long, Y.; Zhu, P.; Wu, F.; Liu, F.; Murugadoss, V.; Winchester, W.; Nautiyal, A.; Wang, Z.; Guo, Z. Recent advances in thermal interface materials. ES Mater. Manuf. 2020, 7, 4-24. doi: 10.30919/esmm5f717.
17. Xu, S. C.; Wang, S. S.; Chen, Z.; Sun, Y. Y.; Gao, Z. F.; Zhang, H.; Zhang, J. Electric-field-assisted growth of vertical graphene arrays and the application in thermal interface materials. Adv. Funct. Mater. 2020, 30, 2003302. doi:10.1002/adfm.202003302.
18. Ci, H. N.; Chang, H. L.; Wang, R. Y.; Wei, T. B.; Wang, Y. Y.; Chen, Z. L.; Sun, Y. W.; Dou, Z. P.; Liu, Z. Q.; Li, J. M.; Gao, P.; Liu, Z. F. Enhancement of heat dissipation in ultraviolet light-emitting diodes by a vertically oriented graphene nanowall buffer layer. Adv. Mater. 2019, 31, 1901624. doi:10.1002/adma.201901624.
19. Lian, G.; Tuan, C. C.; Li, L. Y.; Jiao, S. L.; Wang, Q. L.; Moon, K. S.; Cui, D. L.; Wong, C. P. Vertically aligned and interconnected graphene networks for high thermal conductivity of epoxy composites with ultralow loading. Chem. Mater. 2016, 28, 6096-6104. doi:10.1021/acs.chemmater.6b01595.
20. An, F.; Li, X. F.; Min, P.; Liu, P. F.; Jiang, Z. G.; Yu, Z. Z. Vertically aligned high-quality graphene foams for anisotropically conductive polymer composites with ultrahigh through-plane thermal conductivities. ACS Appl. Mater. Interfaces 2018, 10, 17383-17392. doi:10.1021/acsami.8b04230.
21. Li, X. H.; Liu, P. F.; Li, X. F.; An, F.; Min, P.; Liao, K. N.; Yu, Z. Z. Vertically aligned, ultralight and highly compressive all-graphitized graphene aerogels for highly thermally conductive polymer composites. Carbon 2018, 140, 624-633. doi:10.1016/j.carbon.2018.09.016.
22. Zhang, Y. F.; Han, D.; Zhao, Y. H.; Bai, S. L. High-performance thermal interface materials consisting of vertically aligned graphene film and polymer. Carbon 2016, 109, 552-557. doi:10.1016/j.carbon.2016.08.051.
23. Xu, S. C.; Zhang, J. Vertically aligned graphene for thermal interface materials. Small Strut. 2020, 1, 2000034. doi:10.1002/sstr.202000034.
24. Sun, P. J.; Liu, B. W.; You, Z. Y.; Zheng, Y. M.; Wang, Z. S. Graphene/copper nanoparticles as thermal interface materials. ACS Appl. Nano Mater. 2022, 5, 3450-3457. doi:10.1021/acsanm.1c04080.
25. Xiang, J.; Drzal, L. T. Electron and phonon transport in Au nanoparticle decorated graphene nanoplatelet nanostructured paper. ACS Appl. Mater. Interfaces 2011, 3, 1325-1332. doi:10.1021/am200126x.
26. Yu, Y.; Zhao, Y.; Zhang, X.; Wang, L.; Liao, B.; Pang, H. Construction of a 3D thermal transport hybrid via the creation of axial thermal conductive pathways between graphene layers. Mater. Lett. 2022, 307, 130949. doi:10.1016/j.matlet.2021.130949.
27. Jia, H.; Kong, Q. Q.; Yang, X.; Xie, L. J.; Sun, G. H.; Liang, L. L.; Chen, J. P.; Liu, D.; Guo, Q. G.; Chen, C. M. Dual-functional graphene/carbon nanotubes thick film: Bidirectional thermal dissipation and electromagnetic shielding. Carbon 2021, 171, 329-340. doi:10.1016/j.carbon.2020.09.017.
28. Lv, F.; Qin, M. M.; Zhang, F.; Yu, H. T.; Gao, L.; Lv, P.; Wei, W.; Feng, Y. Y.; Feng, W. High cross-plane thermally conductive hierarchical composite using graphene-coated vertically aligned carbon nanotubes/graphite. Carbon 2019, 149, 281-289. doi:10.1016/j.carbon.2019.04.043.
29. Feng, W.; Qin, M. M.; Lv, P.; Li, J. P.; Feng, Y. Y. A three-dimensional nanostructure of graphite intercalated by carbon nanotubes with high cross-plane thermal conductivity and bending strength. Carbon 2014, 77, 1054-1064. doi:10.1016/j.carbon.2014.06.021.
30. Dai, W.; Lv, L.; Lu, J. B.; Hou, H.; Yan, Q. W.; Alam, F. E.; Li, Y. F.; Zeng, X. L.; Yu, J. H.; Wei, Q. P.; Xu, X. F.; Wu, J. B.; Jiang, N.; Du, S. Y.; Sun, R.; Xu, J. B.; Wong, C. P.; Lin, C. T. A paper-like inorganic thermal interface material composed of hierarchically structured graphene/silicon carbide nanorods. ACS Nano 2019, 13, 1547-1554. doi:10.1021/acsnano.8b07337.

 doi:10.20944/preprints202311.0290.v1

31. Zhang, J. W.; Shi, G.; Jiang, C.; Ju, S.; Jiang, D. Z. 3D bridged carbon nanoring/graphene hybrid paper as a high-performance lateral heat spreader. Small 2015, 11, 6197-6204. doi:10.1002/smll.201501878.
32. Zhang, X. D.; Guo, Y.; Liu, Y. J.; Li, Z.; Fang, W. Z.; Peng, L.; Zhou, J.; Xu, Z.; Gao, C. Ultrathick and highly thermally conductive graphene films by self-fusion. Carbon 2020, 167, 249-255. doi:10.1016/j.carbon.2020.05.051.
33. Peng, L.; Xu, Z.; Liu, Z.; Guo, Y.; Li, P.; Gao, C. Ultrahigh thermal conductive yet superflexible graphene films. Adv. Mater. 2017, 29, 1700589. doi:10.1002/adma.201700589.
34. Song, N. J.; Chen, C. M.; Lu, C. X.; Liu, Z.; Kong, Q. Q.; Cai, R. Thermally reduced graphene oxide films as flexible Lateral heat spreaders. J. Mater. Chem. A 2014, 2, 16563-16568. doi:10.1039/c4ta02693d.
35. Wang, N.; Samani, M. K.; Li, H.; Dong, L.; Zhang, Z. W.; Su, P.; Chen, S. J.; Chen, J.; Huang, S. R.; Yuan, G. J.; Xu, X. F.; Li, B. W.; Leifer, K.; Ye, L. L.; Liu, J. Tailoring the thermal and mechanical properties of graphene film by structural engineering. Small 2018, 14, 1801346. doi:10.1002/smll.201801346.
36. Shen, B.; Zhai, W. T.; Zheng, W. G. Ultrathin flexible graphene film: an excellent thermal conducting material with efficient EMI shielding. Adv. Funct. Mater. 2014, 24, 4542-4548. doi:10.1002/adfm.201400079.
37. Lin, S. F.; Ju, S.; Zhang, J. W.; Shi, G.; He, Y. L.; Jiang, D. Z. Ultrathin flexible graphene films with high thermal conductivity and excellent EMI shielding performance using large-sized graphene oxide flakes. RSC Adv. 2019, 9, 1419-1427. doi:10.1039/c8ra09376h.
38. Teng, C.; Xie, D.; Wang, J. F.; Yang, Z.; Ren, G. Y.; Zhu, Y. Ultrahigh conductive graphene paper based on ball-milling exfoliated graphene. Adv. Funct. Mater. 2017, 27, 1700240. doi:10.1002/adfm.201700240.
39. Li, J.; Chen, X. Y.; Lei, R. B.; Lai, J. F.; Ma, T. M.; Li, Y. Highly thermally conductive graphene film produced using glucose under low-temperature thermal annealing. J. Mater. Sci. 2019, 54, 7553-7562. doi:10.1007/s10853-019-03406-x.
40. Kwon, Y. J.; Kwon, Y.; Park, H. S.; Lee, J. U. Mass-produced electrochemically exfoliated graphene for ultrahigh thermally conductive paper using a multimetal electrode system. Adv. Mater. Interfaces 2019, 6. 1900095. doi:10.1002/admi.201900095.
41. Yang, H.; Zhang, T.; Jiang, M.; Duan, Y.; Zhang, J. Ambient pressure dried graphene aerogels with superelasticity and multifunctionality. J. Mater. Chem. 2015, 3 (38), 19268-19272. doi:10.1039/C5TA06452J.
42. Chen, X. J.; Deng, X. M.; Kim, N. Y.; Wang, Y.; Huang, Y.; Peng, L.; Huang, M.; Zhang, X.; Chen, X.; Luo, D.; Wang, B.; Wu, X. Z.; Ma, Y. F.; Lee, Z.; Ruoff, R. S. Graphitization of graphene oxide films under pressure. Carbon 2018, 132, 294-303. doi:10.1016/j.carbon.2018.02.049.